Surface-directed dewetting of a block copolymer for fabricating highly uniform nanostructured micro-droplets and concentric nano-rings

Richard A. Farrell[†,‡,ϕ,γ] , Nikolaos Kehagias[§], Matthew T. Shaw[χ‡], Vincent Reboud[§], Marc Zelsmann[Δ], Justin D. Holmes[†,‡,ϕ], Clivia M. Sotomayor Torres[§] and Michael A. Morris[†,‡,ϕ,*].

[†]Department of Chemistry, University College Cork, Cork, Ireland, [‡] Centre for Research on Adaptive Nanostructures and Nanodevices (CRANN), Trinity College Dublin, Dublin 2, Ireland. [ϕ] Tyndall National Institute, University College Cork, Cork, Ireland, [§]Catalan Institute of Nanotechnology, Campus de Bellaterra, Edifici CM7, ES 08193 – Bellaterra, Barcelona, Spain, Catalan Institute of Research and Advanced Studies ICREA, 08010 Barcelona, Spain. [χ] Intel Ireland limited, Collinstown Industrial Estate, Leixlip, Co. Kildare, Ireland. [Δ] Laboratoire des Technologies de la Microélectronique (CNRS), 38054 Grenoble, France. [γ] Current address: Department of Chemistry and Biochemistry, University of California Los Angeles, 607 Charles E. Young Drive East, Los Angeles, CA 90095-1569, USA.

RECEIVED DATE (to be automatically inserted after your manuscript is accepted if required according to the journal that you are submitting your paper to)

*To whom correspondence should be addressed Tel: +353·214·902·180; Fax, +353·214·274·197; Email: m.morris@ucc.ie;

ABSTRACT.

Through a combination of nanoimprint (NIL) and block copolymer lithography (BCL), a highly regular dewetting process of a symmetric diblock copolymer (PS-*b*-PMMA, 46-21 kg/mol) occurs whereby hierarchal formation of microdroplets and concentric nano-rings occurs. The process is driven by the unique chemical properties and geometrical lay-out of the underlying NIL fabricated silsesquioxane micro-sized template. Given the presence of preferential substrate-polymer (polystyrene) interactions, directed dewetting can be utilised to produce uniform arrays of micro-sized droplets (diameters of 250 nm to 2500 nm and thicknesses at droplet centre of 30 to 190 nm) of microphase separated PS-*b*-PMMA following thermal annealing at 180 °C. Micro-droplets with diameters greater than 400 nm exhibited a hexagonal close packed (HCP) arrangement of nano-dots on the surface with polydomain ordering except at the periphery where thickness effects (approaching the equilibrium lengths, L_0 of the PS-*b*-PMMA polymer) resulted in cylinders oriented parallel at the edge of the droplet. Furthermore, by increasing the via hole spacer (mesa), it is possible to isolate free-standing, self-aligned and self-supported oblique nano-rings (~250-350 nm) which form as interstitial droplets between the larger micro-droplets. The parallel PMMA cylinders form concentric ellipses, with 2 PMMA cylinders possible, as the thickness is below the natural equilibrium length of the BCP. Optical and magnetic based nanostructures may benefit from such hierarchal organisation and self-supporting/aligned nano-ring templates by combining more than one lithography technique with different resolution capabilities.

KEYWORDS. *Block copolymers, directed-dewetting, nanoimprint lithography, polysilsesquioxane, graphoepitaxy, polystyrene-block-polymethylacrylate, nano-ring, micro-droplet*

MANUSCRIPT TEXT.

Block copolymers (BCPs) are comprised of two or more constituent polymers, tethered together by a covalent bond. Consequently, these polymers when heated above their glass temperature (T_g) and below the order-disorder transition temperature (ODT) will microphase separate and form periodic

nanostructures. Depending on their molar fraction, molecular weight and segmental (Florry-Huggins) interaction parameter, various morphologies such as hexagonal, lamallae or closed packed spherical with critical dimensions ranging from 5 to 50 nm can be formed[1]. When confined as a thin film, the orientation and translational ordering can be perturbed by the close proximity of the substrate and air interfaces resulting in preferred orientations[2,3]. In the case of PS-*b*-PMMA, the PMMA component has a slight preference for the native oxide of a silicon substrate and will wet the surface whilst the PS portion favours the air interface[4]. Thus, this assymetric wetting behaviour leads to the commonly observed island and hole formation where subtle changes in film thickness can dictate the orientation of the PMMA cylinders (parallel versus perpendicular). Furthermore, although the polymer films may have a defined orientation, their translation ordering is limited due the presence of polydomains[5]. Methods for correcting this loss of translational ordering in thin BCP thin films for example include chemical epitaxy of PS-*b*-PMMA[6], graphoepitaxy of PS-*b*-PDMS[7], nano-imprint lithography of PS-*b*-PMMA[8], electric field alignment of PS-*b*-PMMA[3], solvent flow fields[9] and recently reconstructed crystallographic surfaces for PS-*b*-PEO and PS-*b*-PVP[10].

Dewetting instabilities in polymeric thin films are recognized to occur because incompatible interfacial energies between the film and the substrate[11,12]. To date, two different mechanisms for dewetting have been identified; nucleation/growth or spinodal decomposition[13,14] for polymer films. In the nucleation growth mechanism, the film will rupture and the polymer will tend to develop holes which nucleate and ultimately form droplets as a result of Rayleigh instabilities. Alternatively, spinodal decomposition is a dewetting pathway whereby thin films breaks apart through the growth of uniformly distributed surface undulations[13,14]. Factors such as film thickness, polymer-surface interaction, molecular weight, viscosity, and substrate surface tension all play a crucial role in polymer dewetting processes[15].

Recently, researchers have attempted to control this dewetting phenomenon for polymer films by using micro-contact printing (uCP)[16,17] to create microscale chemical patterns. Yoon and co-workers imprinted bilayers of PS and PVP homopolymers using a PDMS stamp followed by a controlled

dewetting process to form ordered micron scale patterns extending towards the millimeter scale[18]. The authors were able to induce a thickness variation as a result of the imprinting process which facilitated controlled dewetting and a partial layer inversion after thermal annealing of the arrays. Homopolymer films of polystyrene (PS) and poly(4-vinyl pyridine) (P4VP) containing Rhodamine 6G (Rh6G) were also controllably dewetted on line and via hole topographic pre-patterned substrates to create ordered nanopatterns of spherical caps[19]. The resultant caps (~70 nm) were considerably smaller than the template used (200 nm) representing a resolution enhancement of ~300%. Alternatively, 2-dimensional arrays of square pillars can be utilized to control the dewetting behaviour of polystyrene microdroplets with diameters ranging from 1-20 micron, depending on the initial thickness of the film when exposed to a solvent vapour[20]. The authors noted that substrate pattern was crucial in controlling parameters such micro-droplets size (1-2 orders magnitude range) and that polymer films with thickness below 40 nm always produced defect free droplets arrays which occupied the interstitial sites (between two via holes) whilst films greater than 40 nm displayed uncorrelated wetting behaviour with the underlying topography.

Block copolymers thin films are also prone to dewetting instabilities. Moreover, the interplay between the quantized film thickness and the intrinsic polymer length scale, the tendency for one of the blocks to preferentially wet an interface (i.e. asymmetric and symmetric wetting) and the possibility of autophobic dewetting make these systems more interesting for understanding and controlling dewetting processes[15,21-23]. Carvalho and co-workers investigated the stability of a triblock copolymer PS-PEB-PS (polystrene cylinders in a poly(ethene-co-butene-1)) during drying on planar mica surfaces[24]. Aperiodic arrays of parallel ribbons (~20 nm height, 150-500 nm wide) and hexagonal arrays of droplets (~30 nm height, 500-600 nm wide) were formed on planar surfaces as a result of fingering instabilities. The linear ribbons and hexagonal droplets displayed microphase separation with the cylinders adopting parallel orientations (with respect to the substrate) for both droplet and ribbon formation. The ribbon patterns displayed uni-direction ordering as they frequently followed the topography of the mica surface. Croll has also demonstrated the ability to control the droplet shape by modifying the internal

structure of the droplet using PS-*b*-PMMA block copolymers[25]. In the isotropic state, the droplet assumed a spherical shape whilst after thermally annealing, it transitioned to the anisotropic state; hence the droplet became terraced ultimately adopting a hyperbolic profile as a result of microphase separation. The authors suggested that two competing actions led to the hyperbolic structure; edge tension and edge repulsion[25,26]. Hierarchal nano-web nanostructured block copolymer arrays can also be fabricated by utilising the fingering instabilities associated with a block copolymer on a substrate in a restricted geometry by placing a spherical lens in close proximity to it[27]. Subsequently concentric serpentine structures are formed on the macroscale whilst further exposure to a solvent facilitates microphase separation of the PS-*b*-PMMA on the nanoscale with cylinders oriented perpendicular to the substrate. The majority of droplet formation by controlled dewetting processes has to date, been carried out on planar surfaces. PS-*b*-PEO films are recognized to dewet the substrate during solvent annealing because of small changes in the interface chemistry of the solvent swollen film and the substrate[28]. Using this dewetting to their advantage Kim *et al*.[29] used this behaviour to form hierarchal structures by intentionally dewetting a PS-*b*-PEO film on pre-patterned SAM surfaces manufactured by micro-contact printing techniques. The PS-*b*-PEO films simultaneously undergoes microphase separation and dewetting when swelled in a benzene atmosphere. By directing the dewetting process, the authors were able to fabricate convex lens shaped caps over 1mm^2 regions with extremely high regularity.

Nanoimprint lithography is a top-down parallel lithographic technique capable of creating patterns with sub 10 nm resolution[30] by mechanically deforming a polymeric resist layer in conjunction with a thermal[31] and/or ultra-violet curing step[32]. The resulting profiles are ideal for subtractive pattern transfer into the underlying layer or alternatively, deposition within the profiles followed by a lift-off step. This technique can be extended to inorganic polymer systems such as poly-silsesquioxanes (PSSQ) for fabricating nano-arrays and 3D structures[33]. Silsesquioxane nanostructures have found uses in many applications recently, most notably as a direct write negative tone electron-beam resist for patterning nanowires[34], low dielectric constant materials[35], and structures for 3D photonic materials[36]. Nanoimprint lithography can also be used to control orientation and translational ordering within a block copoylmer

film by directly imprinting the polymer during microphase separation. Li *et al*. were first to show that asymmetric PS-*b*-PMMA (thickness ~ 1 L_0) films could be imprinted when deposited on neutral PS-*r*-PMMA brush layers[8]. Moreover, it was possible to create both cylinders perpendicular and horizontal to the plane with improved translational ordering by adjusting the thickness of the films.

Previous work on aligning block copolymer nanopatterns (by graphoepitaxy) within electron beam patterned hydrogen-silsesquioxane (HSQ) type templates have shown that line and concentric hexagonal arrays of PS-*b*-PMMA lamallae patterns can be assembled with precision[37]. The combination of using a neutral brush layer at the base and a hydrogen silsesquioanxe (HSQ) sidewall allowed the researchers to create hexagonal arrays of parallel cylinders and concentric rings of 1-2 PMMA cylinders with low defect content. Extremely thin layers (~ 2 nm) of hydrogen silsesquioxane have also been written by electron beam methods to create chemical patterns (14 nm half-pitch) to align and register PS-*b*-PMMA patterns[38]. More importantly, sparse chemical patterns of these HSQ lines with spacers double, triple and quadruple that of the natural periodicity of the BCP, were shown to direct the self-assembly of the nanopatterns, thus representing a resolution enhancement of up to 4 when combined with the top-down exposure techniques[38]. Concentric rings were also possible using this approach, with the authors highlighting approximately 140 concentric PMMA rings could readily be fabricated without any discernible loss in translational ordering. Although direct write exposure of HSQ patterns have yielded well-aligned linear and concentric ring structures of PS-*b*-PMMA structures, electron beam patterning of HSQ is expensive and in the case of HSQ, challenging[39].

Block copolymers because of their flexibility can be fashioned into nano-ring structures by graphoepitaxy[40] and chemical patterning[38,41]. Ferromagnetic nanostructures which have a ring structure are of interest because they have stable magnetic states (onion and vortex) at remanence and as a result, may find uses in magnetic RAM applications[42]. Nano-ring structures have recently been reported for PS-*b*-PMMA[41], PS-*b*-P4VP[43,44] and PS-*b*-PFS-*b*-P2VP[40] block copolymers either by tuning the hydrophobicity (no placement) or by implementing chemical/physical pre-patterning techniques. Chung *et al*. have used graphoepitaxy to create single and up to 5 concentric circular ferromagnetic cobalt rings

by availing of aligned PS-*b*-PDMS structures as the BCP provided a significant etch contrast enhancement with respect to other BCPs[45]. The researchers investigated the effects of confinement diameter and commensurability as a function of increasing concentric rings (1-5 rings) for the block copolymer system.

Herein patterned poly-silsesquioxane (PSSQ) films with varying dimensions of via hole and linear arrays have been fabricated using an ultra-violet nanoimprint lithography (RUVNIL[33]) technique to investigate the self-assembling properties and polymer flow/dewetting phenomena of cylinder forming polystyrene-block-polymethylacrylate (PS content 0.72, 67.0 kg/mol) block copolymer films following thermal annealing. Directed dewetting can be utilised to produce uniform arrays of micro-sized droplets where the PS-*b*-PMMA polymer simultaneously undergoes microphase separation, de-wets the methylated surface and flows into via holes to minimize its surface energy during thermal annealing at 180 °C. The droplet size was readily controlled by adjusting the pitch and via hole dimension which circumvented droplet merging. In addition, we also show that it is possible to fabricate isolated concentric nano-ring structures with 2 PMMA cylinders (250 - 350 nm) which form between the larger micro-droplets without the need for extreme confinement and avoiding expensive lithographic techniques.

RESULTS & DISCUSSION.

Nanoimprinting of a silsesquioxane thin film presents the opportunity to access its unique chemical (methylated surface) and photo-patternable properties whereas conventional patterning techniques which employ post plasma processing (surface oxidation) do not. Line and via holes arrays with spacer and critical dimensions ranging from 200 nm up to 4000 nm (mesa and trench were approximately equal in lateral dimensions) were created in SSQ inorganic polymer films using a RUV-NIL process. Briefly as outlined in figure 1a-i, the inverse metallic patterns of the desired lay-out and dimensions were first created on a transparent quartz substrate. Subsequently, a sacrificial polymer layer was deposited prior

to the PSSQ deposition to ensure effective release after UV exposure. The Pyrex/metallic template/sacrificial polymer/polysilsesquioxane stack was brought in contact with the silicon substrate and imprinted for 60 second at 6 bar whilst simultaneously exposing to a UV source to ensure cross-linking of the silsesquioxane. Finally the stack and the silicon substrate were released and the PSSQ developed in TMAOH resulting in the formation of the topographic PSSQ patterns. Top-down SEM images of the patterned PSSQ structures on brush-coated silicon substrates are shown in figure 1-j&k. The fidelity of the pattern transfer from the RUV-NIL process was not of strict importance for the current study as only via holes were required to act as guides. A residual layer of approximately 100 nm remained from the imprinting process whilst the resultant line and via hole patterns had significant rounding (supporting info figure S1 b & e). Figure 1-l is an image of water droplet residing on a planar PSSQ surface. Contact angles for the planar PSSQ films ranged from 96 ° to 107 ° highlighting the extent of surface methyl (-CH_3) groups present on the surface. The hydrophobic surface was essential for creating periodic micro-scale droplets.

Figure 2 highlights the importance of the type of interface between the substrate and block polymer as this interaction ultimately influences the cylinder orientation for the asymmetric PS-*b*-PMMA and more importantly, limits the ability to form a continuous and nanostructured film. Analysis of the asymmetric PS-*b*-PMMA block copolymer nanopatterns on silicon (native silicon dioxide) surfaces revealed the well observed phenomenon of island and hole formation (figure 2-a)[46]. The PMMA (surface tension, γ_{PMMA} = 41.1 mNm) has a strong preferential interaction for the polymer/substrate interface as it has a lower surface energy copolymer component whilst the PS (surface tension, γ_{PS} = 40.7 mNm) component favours the polymer/air interface[47,48]. Figure 2-a is a 3D rendering of a 2x2 micron AFM tapping mode image for an asymmetric PS-*b*-PMMA block copolymer deposited from a 1% weight solution on a native silicon dioxide surface. FFT measurements reveal that the periodicity (natural equilibrium distance, L_0) is ~ 40 nm which agrees well with previous literature findings for assymetric PS-*b*-PMMA with a M_W of 67k g/mol [49,50]. As a result of subtle surface tension variation between the two blocks, a PMMA wetting layer forms at the silicon interface, PMMA

cylinders align parallel to the substrate and polymer islands form to minimise energy so as to be commensurate with the natural periodicity of block copolymer. Under asymmetric wetting conditions, the thickness of block copolymer films becomes quantized as the film wants to be commensurate with these quantized thickness values. Asymmetric wetting conditions follow a rule which dictates that a thickness of nL_0 + 0.5 times the natural equilibrium length must be satisfied. For a 1 % weight concentration, polymer islands form where the thickness satisfies this condition and the PMMA cylinders form fingerprint patterns. As the film thickness is extremely thin, polymer in the hole sections is too thin (i.e. < 1 L_0) and therefore, no nanopatterns are formed within these regions.

By grafting a random copolymer (neutral with respect to PS and PMMA) to the native silicon oxide, the PMMA affinity for the native silicon oxide surface can be decoupled and allow the microdomains to orient normal to the substrate (figure 2-b)[51-53]. Consequently, a uniform film of PMMA cylinders in a PS matrix (film thickness ~ 50 nm) can be assembled on a neutral brush layer after annealing at 180°C under vacuum for 24 hour from a 1% weight solution. The natural cylinder to cylinder in-plane repeat distance was determined to be 40 nm (SD 3.5 nm) with cylinder diameter of approx 20 nm from SEM and AFM (FFT calculations). Similar L_0 values were also measured for other studies involving assymetric PS-*b*-PMMA with a M_W of 67k g/mol[50,54-56]. PS-*b*-PMMA microdroplets were exposed to a oxygen/tri-fluoromethane (O_2/CHF_3) reactive ion-etch to partially remove PMMA for SEM imaging purposes.

PS-*b*-PMMA films on non-imprinted PSSQ surfaces were found to function quite differently to the previous two surfaces. Under similar thermal and preparation conditions, neither PS nor PMMA segments favourably wet the highly methylated PSSQ surface and consequently gave rise to non uniform and random droplet arrays with sizes ranging from the sub 100 nm to well beyond the micron scale (figure 2-c and d). Figure 2-c displays a tilt SEM image of a large droplet (> 2 micron) which has undergone microphase separation but has also dewetted the surface and formed large uncontrollably globular-like structures. In other regions (figure 2-d) the polymer can be seen to form smaller droplets with sizes ranging from 20 nm to 100 nm highlighting the randomness of the dewetting process on the

PSSQ surface. Surface dewetting is to be expected as surface tension values for PSSQ (>20 mNm[57]) are quite different to that of the PS and PMMA.

Our motivation for the following study developed from frequently observing the formation of micro-droplets on planar PSSQ substrates (figure 2-d) and in some cases, self-supporting nano-rings from our investigations relating to aligning PS-*b*-PMMA nanopatterns by graphoepitaxy (figure 2-e and supporting information section S1) techniques on these PSSQ physical patterns. The inaccessibility to the brush layer owing to presence of the residual layer and rounding of the PSSQ profile limited these investigations. Consequently residual polymer located on mesas during graphoepitaxy studies has prompted recent work on reducing the mesa itself to very small dimensions[58] or replacement with sparse pillars with feature sizes similar to that of the BCP.[45]

As highlighted in figure 3, chemical interactions between the substrate and block copolymer are important for controlling the continuity and orientation of the film. With this in mind and the knowledge of droplet formation during graphoepitaxy experiments, we found that it was possible to localise these structures in desired locations across via hole arrays. By depositing 1% weight solutions of PS-*b*-PMMA (46-21 kg/mol) on PSSQ via hole arrays and annealing at 180 °C for 24 hr, a highly regular dewetting process was found to transpire. Optical microscopy analysis (figure – 3a and 3b) confirms that the dewetting process is extremely effective and extends well beyond the 50 micron scale. On closer inspection, each microdroplet (orange only) is surrounded by 4 via holes (orange with black ring).

The block copolymer has undergone microphase separation and nanostructured topography can be observed for all micro-droplets on the mesas and polymer within neighbouring via holes. For our investigations, rather than adjust the BCP weight percentage, the via hole spacer and occasionally the via hole dimension were varied to control the dewetting process. Figure 3-c displays a SEM image of the micro-droplet formation on the PSSQ pattern. In this instance, the 610 nm spherical micro-droplets (figure 3-d) are precisely positioned within the centre of each 1100 nm transverse mesa with a nearest neighbour distance of approximately 700 nm. During thermal annealing the as-deposited film ruptures

due to non-favourable wetting between both PS (surface tension, γ_{PS} = 40.7 mNm) and PMMA (surface tension, γ_{PMMA} = 41.1 mNm) with the PSSQ (surface tension, γ_{PSSQ} < 20 mNm) substrate and acts to minimize surface energy by producing micro-droplets. The hydrophobic PSSQ template, or more importantly the via hole structures, act as guides to direct the formation of this dewetting progression while simultaneously sequestering polymer in the via holes (figure 3-e) during dewetting as a result of capillary forces. As the surface is extremely methylated (as observed from contact angles of approximately 100°), the majority PS component preferentially wets the fully crosslinked PSSQ surface resulting in a symmetric wetting regime. Recently, similar studies by Suh *et al*. confirm that when silsesquioxane surfaces are fully cured at 400 °C, the PS tends to wet the PSSQ surface rather than the PMMA[59]. Figure 3-f and g are tilt SEM images captured at 70° which provide 3D topographical information on both the droplet and surplus polymer in the via hole. The microdroplets form the spherical cap-like structures with the polymer within the via hole forming an inverse cap, to compensate for the rounded profile of the via hole from the RUV-NIL process.

Microdroplet sizes ranging from *ca*. 400 nm to 2500 nm (figure 4 a-f) can easily be tuned by adjusting the dimensions of the physical pre-pattern prior to polymer deposition. Figure 4 examines droplet shape, topographic structure and cylinder orientation as microdroplet diameter is reduced from 2000 nm to 500 nm. Figure 5 provides additional information on droplet height at the centre and at the edge by cross sectional dual beam analysis to assist in postulating orientation and thickness effects within the droplets. Thus far, we have neglected to comment upon the orientation of the block copolymer at the surface and within the substructure of the droplet. Firstly, we begin by analysing the topographic nanostructure as function of decreasing droplet size. Figure 4-b and c are top down and tilt SEM images for a 1550 nm microdroplet. Although the microdroplet is well phase separated, a polydomain hexagonal close packed (HCP) arrangement of 20 nm sized holes is observed across the surface with the presence of more ordered domain located towards the centre of the droplets as radius of curvature is negligible. Defects and cylinder re-orientation become more pronounced as the droplet thickness approaches monolayer values (symmetric wetting condition, i.e. $T_{droplet} < L_0$ of 40 nm) at the periphery of the droplet. This is

confirmed by analysing centre to centre spacings for various droplet diameters (figure 4-g). For simplicity, we confine these measurements to the centre of the droplets as extracting centre to centre spacings is not possible at the edge (refer to supporting information section 3). The average periodicty (L_0) of the PS-*b*-PMMA (67k g/mol) thin film is approximately 40 nm and depending on droplet size, the value decreases to 34 nm as droplet diameter changes from 1800 to 600 nm. Such deviation in the centre to centre spacings is to be expected owing to deterioration of the hexagonally closed packed arrangement (5 and 7 member)

polydomains as a results of increased defects near the edge of the micro-droplet. The orientation of the PMMA cylinders within the micro-droplet is perturbed with cylinders in some cases, tending to favour parallel orientations to the substrate when at the perimeter of the micro-droplet as the film thickness is sub 1 equilibrium repeat distance (< 40 nm). Defect density tends to increase drastically as one approaches the droplet edge as the radius of curvature becomes greater and thickness effects become more important. It is well accepted that subtle changes in film thickness can result in abrupt changes in film orientation. Such behaviour has previously been shown for changing film thickness with PS-PI droplets although annealing was performed by solvent vapours[60]. Interestingly, polymer within the actual via hole (figure 4-g) was microphase separated, although the polymer structure within the via hole is significantly perturbed with cylinders oriented in both parallel and perpendicular orientations. The mixed morphology can be attributed to subtle changes in droplet thickness caused by the rounded profile of the via hole.

Focus ion beam (FIB) cross sectioning was employed to ascertain thickness values of the droplet as a function of microdroplet diameter. Figure 5a-c displays 54° tilt SEM images post FIB cross sectioning of a 640 nm, 1000 nm and 2580 nm droplets respectively residing above the 400 nm PSSQ film. To ensure preservation of the microdroplet during the physical etch process, platinum layers were first deposited by electron beam followed by ion beam techniques. Such is the fine polish created by this technique, any chance of observing the internal nanoscale structure of the droplet is prohibited as the etch essentially creates a fine polish at the interface. The micro droplets adopt a convex, spehrical cap

shape which is prevalent across all microdroplet diameters. It was found that droplet thickness at the centre (h) scales as a function of droplet diameter (Ø) where the droplet height was approximately 10% of the droplet diameter as highlighted in figure 5-d. Closer inspection of the thickness at the droplet edge reveals that the thickness is well below an L_0 of 40 nm. Why do cylinders lie parallel?.

For the PS-*b*-PMMA droplets on the PSSQ surface, simply sectioning through a droplet with FIB restricted our ability to observe substructure orientation, whereas topographic imaging of the droplets was achieved by introducing a partial etch of surface PMMA domains. Kim *et al*.[29] highlighted that the structure of a micro-droplet consisting of assymetric PS-*b*-PEO which predominantly forms a hexagonal closed packed arrangement of cylinders in a continuous and uniform film had undergone a phase transition to a spherical structure. The authors suggested that either significant swelling of the PS domain by benzene or by the presence of a packing frustration owing to the inherent radius of curvature of the droplet led to the phase transition. As our microphase separation technique is realised by thermal annealing under vacuum conditions, domain swelling is an unlikely event. In figure 6, we have attempted to investigate the sub structure by simple scribing techniques. Although the method provides more detail of the internal structure, it is limited by the fact that such a technique creates shear and tensile forces during breaking the underlying PSSQ film (and silicon substrate) and causes significant deformation (uncontrolled tearing) of the microdroplet. In some regions (figure 6-a-d), some spherical features clsoe to 20 nm are observed but since no large polydomain (repetition of features, periodicity) behaviour is evident, we cannot categorically conclude whether cylinders with a defined orientation exist or if it is in fact, a structure where a phase transition from hexagonal to spherical has transpired.

By extending the mesa widths to larger dimensions and as a consequence of the unique geometry of the top-down (via holes) and bottom-up (microdroplets) structures, oblique nano-rings whereby the PMMA cylinders produced concentric rings parallel to the substrate are formed. Figure 7-a-d displays tilt SEM images for two different pitch and via hole spacings of the PSSQ pre-patterns and the resultant microdroplets. Beyond via spacer dimensions of ~ 1.4 microns as highlighted in figures 7-b and 7-d, it is possible to create self-aligned, self-supporting nano-rings with dimensions ranging from 250-350 nm

with preferred cylinder orientations. At this stage, the microdroplet also begins to adopt an octagon shape which can probably be attributed to the method of film rupture during dewetting. Annealing the block copolymer films for 24 hr provides adequate time for the mass flow of the BCP to form the microdroplet arrays. Figure 7e highlights a structure formed during 6 hr of annealing. Insufficient time has elapsed for the microdroplet array to form. However, the image does provide insight into the dewetting mechanism and how nanorings form as a result of this process. Polymer around the via hole flows in equally into the via. As two via holes pull polymer into the hole (whilst polymer also moves to the interstitial mesa sites), a thin ridge forms between two via holes until it completely disappears. If the distance for polymer flow is too great, then polymer will be left behind to form a droplets as will and ultimately, nanorings.

The elongated nano-rings self-align with their long axis parallel to the two nearest microdroplets and orthogonal to adjacent via holes (indicated by white arrows in figure 7-e). The registration of the nano-rings to neighbouring microdroplets and via holes have an error of placement of ~ 10% as highlighted in figures 8a and 8b. The droplets long axis runs orthogonal to the via hole to via hole direction with some droplets deviating from this direction by no more than 15°. In most cases, the droplet registers with both the via hole and microdroplet. Regrettably the process was not homogeneous across the entire via hole structures as nano-rings did not develop in all available sites (figure 7-b). The process of forming microdroplets (which subsequently form nano-ring structures) at all available sites requires precise delivery of polymer to all sites, strict control over variables such as temperature and the physical prepatterns but most importantly, the reliance of the adjacent microdroplets to adopt precise positions and shapes.

Further examination of the nano-rings in figure 8a-c reveals that the PMMA cylinders form aperiodic ring structures arranged parallel to the substrate within the PS matrix. The natural periodicity (L_0) for parrallel cylinders of ~ 40 nm cannot be sustained as the film thickness varies across the nano-ring. Extrapolating the droplet thickness for a 300 nm droplet from figure 6-c, suggests most of the

droplet thickness is sub monolayer (below L_0). As previously determined, cylinders are oriented parallel to the substrate and the PS component wets the PSSQ interface. The outer PS segment has the highest repeat distance of 53 nm as film thickness changes are most pronounced at the edge. The next repeat distance of 34 nm is considerably smaller than the natural periodicity whilst the internal PS core has a radius of 49 nm.

CONCLUSION

PSSQ pre-patterns made possible by NIL which combine chemical and physical properties are extremely useful substrates for controlling dewetting processes and ultimately, the formation of hierarchal structures. Tunable microdroplet arrays with droplet sizes ranging from 250 nm to 3000 nm can be fabricated with relative ease by pre-programming the PSSQ via hole dimensions. Although the microdroplets are microphase separated, the ordering of the hexagonal closed packed arrangement on the surface is limited by droplet thickness and radius of curvature. The radius of curvature of the droplet itself may also cause a cylinder to spherical domain transition but such a transition ultimately requires more advanced microscopy investigations (HRTEM/staining). Directional, self-supporting (template free) and self-aligned nano-rings are produced when microdroplets are placed beyond a critical distance (1.4 micron). The droplets adopt an aperiodic polydomain structure as the radius of curvature is pronounced. Future work will involve precision template fabrication by NIL to create square trench and via hole profiles whilst work will also centre on delivering controlled amounts of polymer to the substrate to ensure nano-ring formation is continuous and each interstitial site is occupied. By utilising both the trench and the mesa surface regions, it is possible to envision using this graphoepitaxy approach for fabricating high density arrays of nano-ring structures for magnetic memory applications by minimising mesa spacings and creating droplets below 300 nm.

ACKNOWLEDGMENT

The authors would like to acknowledge the following sources of funding which supported this work: SFI grant *03-IN3-I375*, SFI CRANN CSET grant and NapaNil EU NMP FP7. The authors are grateful to Robbie Dunne, Marie Brennan and Siobhan Lally at Intel Ireland for access to microscopy facilities and continuous support. Access to fabrication facilities (plasma processing) was partly funded by the SFI National Access Program at the Tyndall National Institute (Project Number 132). We thank Vladimir Djara for support with pattern transfer techniques.

EXPERIMENTAL SECTION

PSSQ Substrate fabrication and RUV-NIL: The synthesis of the UV-curable poly-silsesquioxane (PSSQ) is reported elsewhere[61]. Polyhedral Silsesquioxane (PSSQ) cages bearing 8 dimethylsilyloxy groups were functionalized with polymerisable groups by a hydrosilylation reaction carried out on the Si-H functional group. A polyhedral silsesquioxane with a 6 alkyl chain length with a viscosity of 0.9 Pa.s in toluene was used for all RUV-NIL experiments. Resist patterns were created on a quartz substrate by electron-beam lithography (Zeiss Supra 40/Raith system) using PMMA. Chromium was evaporated on to the the opened resist patterns by electron beam evaporation (Temescal 2000F) and the finalised chromium patterns realised by lift-off. A sacrificial polymer LOR (MicroChem Corp) was deposited at 3000 rpm on top of the metal arrays to enable effective release after imprinting. The mask was completed by spincoating the PSSQ onto the sacrificial polymer at 1500 rpm . The mask layer was imprinted onto a brush coated 30 x 30 mm silicon substrate. The brush was a 1 % weight solution of random copolymer of polystyrene-polymethylacrylate (PS-*r*-PMMA) with a polystyrene content of 58 % and was purchased from Polymer Source of Quebec, Canada. PS-*r*-PMMA was grafted to the silicon substrate by spincoating at 4000 rpm, annealing the thin film at 180 °C (48 hr) under vacuum and removing the excess polymer by repeated immersion in toluene three times under sonication. A reverse ultra-violet nano-imprint lithography (RUV-NIL) technique was employed to fabricate the PSSQ templates using a 2.5 inch Obducat nanoimprint system under a pressure of 6 Bar for 60 second followed by a 5 second UV polymerisation (λ = 250 - 400 nm) step to cross-link the siloxane structure.

Development of the PSSQ was performed in 0.1 molar tetrametylammoniumhydroxide (TMAOH) for 2 minute and rinseed under flowing de-ionised water for additional 2 minute. All spincoating was performed on a Speciality Coating Systems G3P-8 spin-coater.

Deposition and thin film formation: Polystyrene-*block*-polymethylacrylate (PS-*b*-PMMA) with a polystyrene content of 0.72 and a M_n value of 67.0 kg/mol was purchased from Polymer Source Inc. of Quebec (Canada) and used as received. 1 wt.% PS-*b*-PMMA in toluene solutions were spin coated using a Speciality Coating Systems G3P-8 spin-coater at 3000 rpm onto the patterned PSSQ films. Simultaneous microphase separation and dewetting was achieved by placing the films in a vacuum oven for 24 hour at 180 °C. For planar films where hexagonal cylinders of PMMA were oriented perpendicular to the substrate, a random copolymer of polystyrene-random-polymethylacrylate (PS-*r*-PMMA) with a polystyrene content of 58%, was grafted to the silicon substrate by annealing a film at 180 °C for 48 hour under vacuum. Non-grafted random copolymer was subsequently stripped from the substrate by washing in toluene 3 times.

Thin film and micro-droplet characterisation: SEM images were obtained using Hitachi S4800 and FEI strata dual-beam 235 microscopes operating at 2-5 kV. To improve SEM contrast, partial removal of the PMMA was performed by dry etching with an Oxford plasmatech 100 using oxygen/tri-fluoromethane (O_2/CHF_3) mixture for 20 seconds at a base pressure of 0.1 mTorr at 10 °C. Loss of PS was negligible in comparison to the PMMA and the etch rate for PMMA was 25 nm per minute. In order to minimize charging effects, samples were coated with a thin layer of Au/Pd deposited by sputtering methods. FIB cross-sectional samples were prepared using a FEI strata dual-beam 235 system. Contact angle measurements were determined on a DataPhysics OCA30 system operating in static mode according to the sessile drop method. Optical images of the polymer microdroplet arrays were recorded on a Zeiss Axioskop 40 Pol Optical Microscope.

FIGURE CAPTIONS

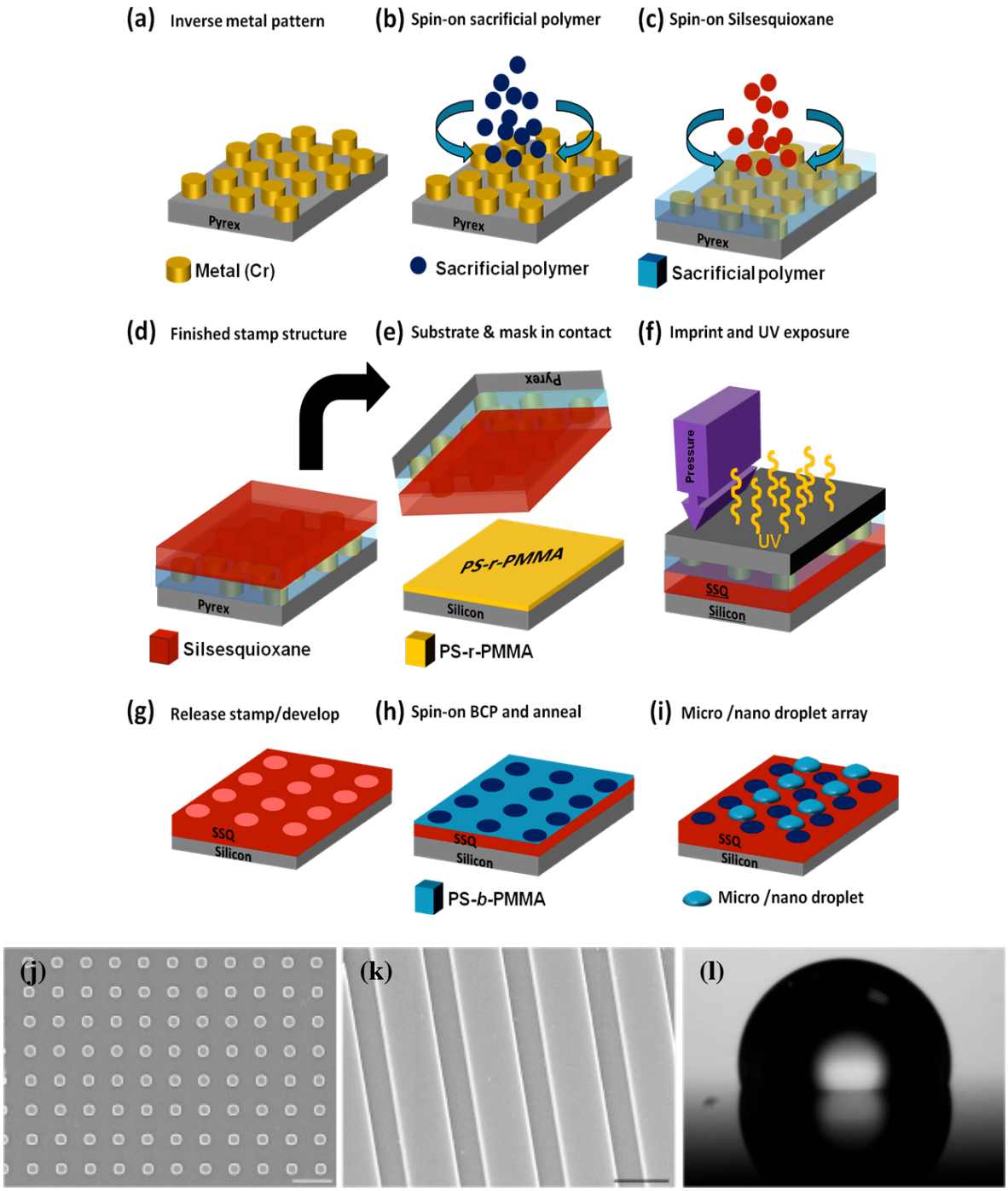

Figure 1: (a)-(i) schematic 3-D diagram process flow for creating patterned PSSQ films by RUV-NIL technique. Top down SEM images of NIL prepared PSSQ (j) via hole arrays and (k) line arrays prior to block copolymer deposition and dewetting and (l) Optical image of contact angle ~ 100 ° measured on a planar PSSQ surface post UV curing. The scale bars in images (j) and (k) are 2 micron and 1 micron respectively.

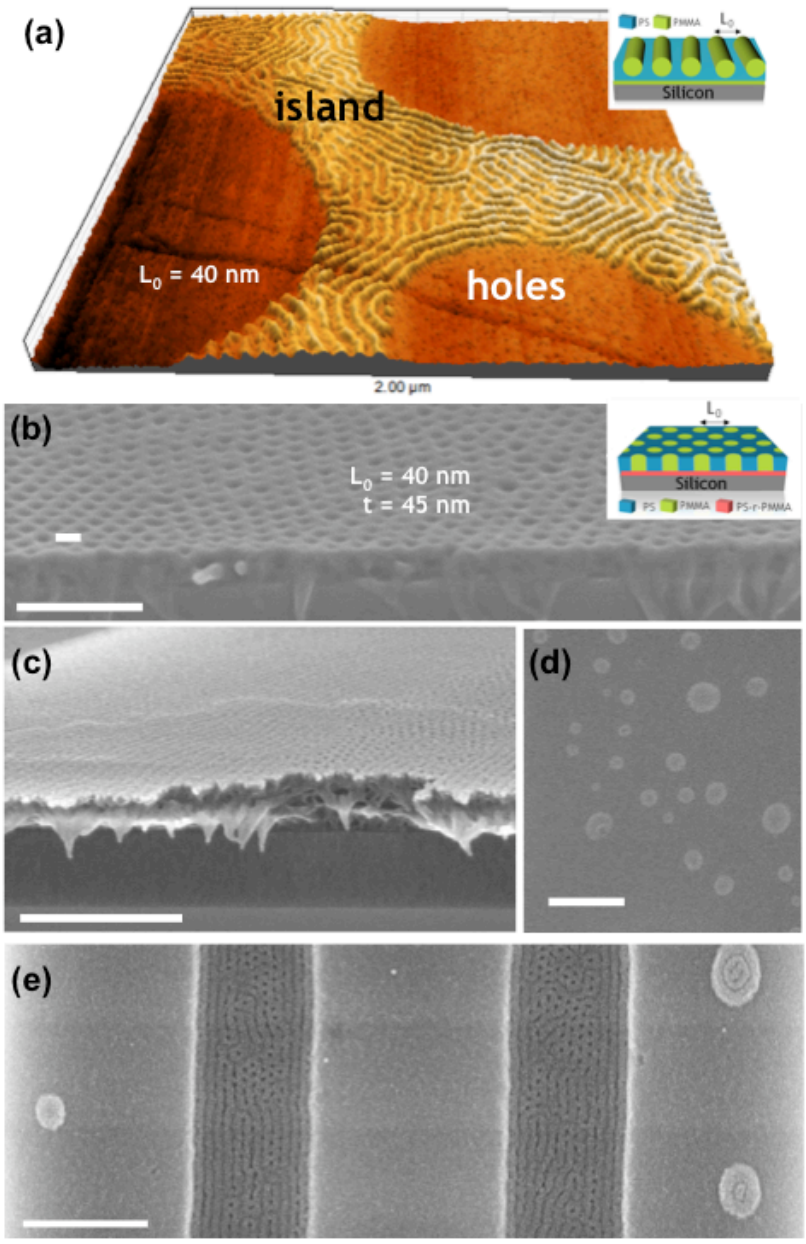

Figure 2: PMMA cylinder orientation (a) 3D AFM tapping mode image (z-height 65 nm) of the island and hole formation for a 1% wt. PS-***b***-PMMA (46-21 kg/mol) on native silicon dioxide where cylinders are arranged parallel to substrate, (b) 70° cross sectional SEM tilt image of a PS-*b*-PMMA (46-21 kg/mol) deposited from a 1% wt. solution on ~ 5 nm PS-*r*-PMMA which is chemically grafted to the native silicon dioxide where cylinders are arranged perpendicular to substrate, (c) 70° cross sectional SEM tilt image of large droplets of PS-*b*-PMMA after dewetting on an PSSQ surface, (d) top-down SEM image of small droplets PS-*b*-PMMA after dewetting on an PSSQ surface and (e) non- alignment of PS-*b*-PMMA nanopatterns in patterned arrays of PSSQ with nano-ring formation on the mesas. Scale bar values are as follows; (b) 200 nm, (c) 500 nm, (d) 200 nm and (e) 450 nm.

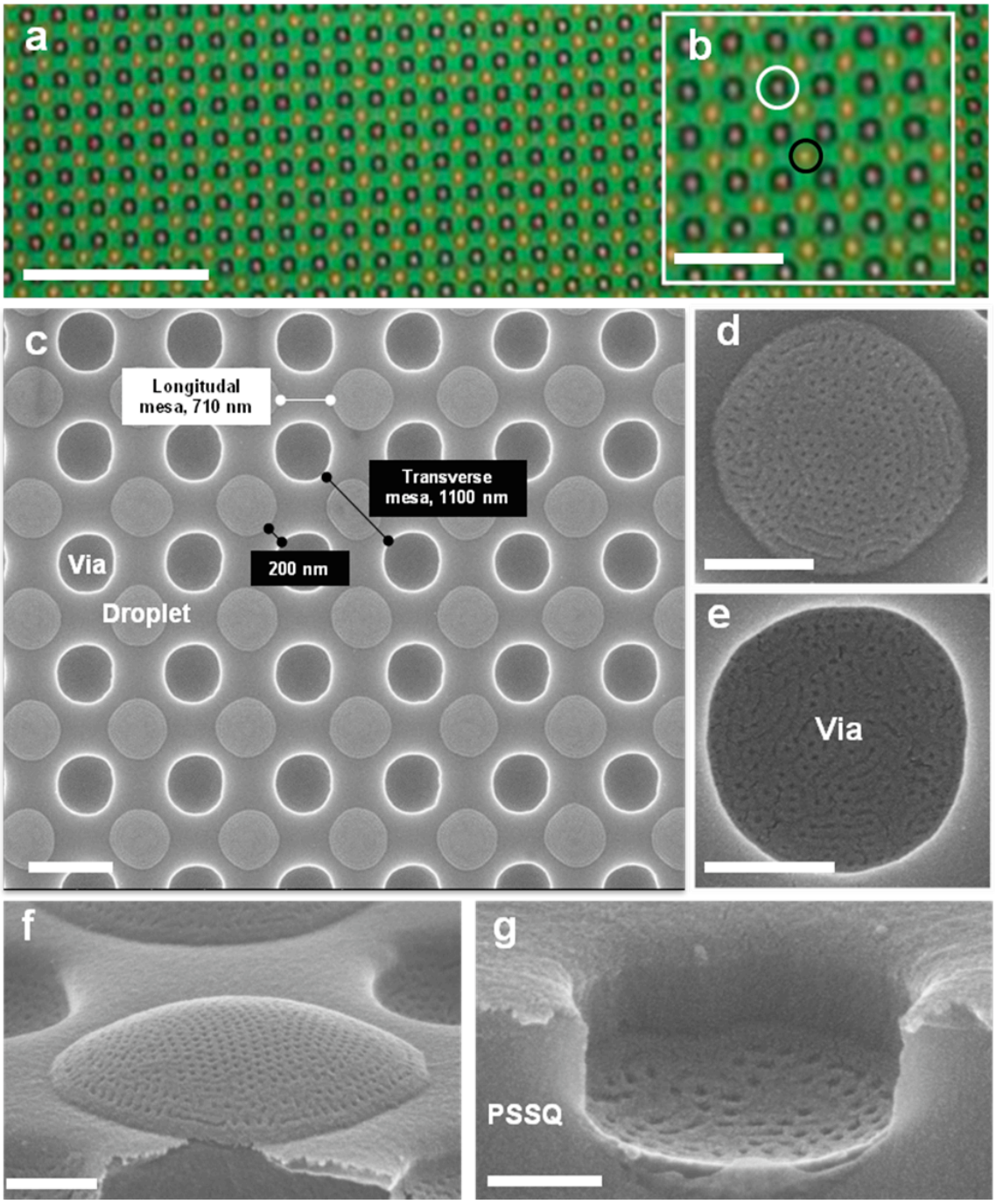

Figure 3: (a), (b) Optical microscopy and (c) SEM images of an extremely regular array of ~ 675 nm micro-droplets forming atop of the transverse mesas between the 600 nm via holes as a result of dewetting processes for a 1% wt. PS-PMMA (46-21 kg/mol) (d) and (e) SEM images of microphase separation within the micro-droplet on the mesa and within the via hole (reservoir) taken from image d. (f) and (g) 70° tilt SEM images of microphase separation within a micro-droplet on PSSQ mesas and via holes. The scale bars are as follows: (a) 10 micron, (b) 4 micron, (c) 1000 nm, (d) 300 nm, (e) 300 nm, (f) 250 nm, (g) 150 nm.

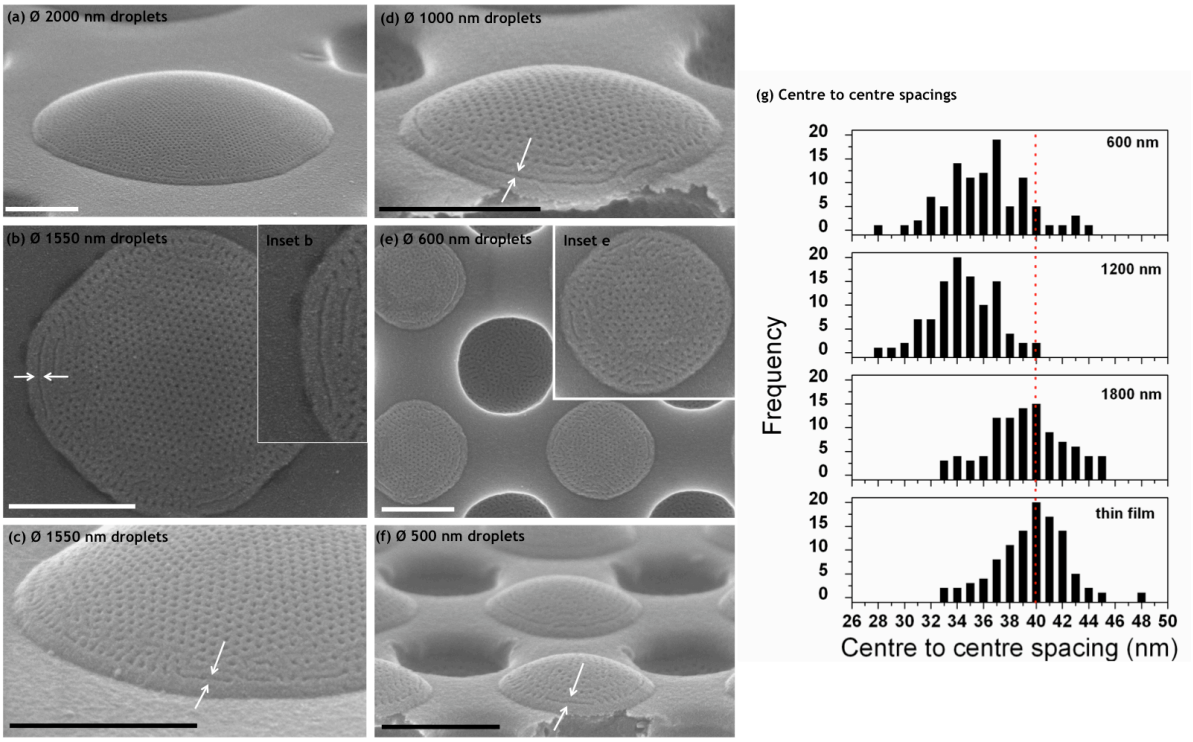

Figure 4: Topographic structure with changing droplet size. SEM top down and 70° tilt images for (a) 1550 nm droplet and (b) 600 nm droplet and tilt 70 ° SEM images for (c) 2000 nm droplet, (d) 15500 nm droplet (e) 1000 nm droplet and (f) 500 nm droplet. White arrows indicate parallel cylinder formation. The scale bars are 500 nm for all images. (g) Centre to centre spacing distributions for a thin film, 1800 nm, 1200 nm and 600 nm micro-droplet.

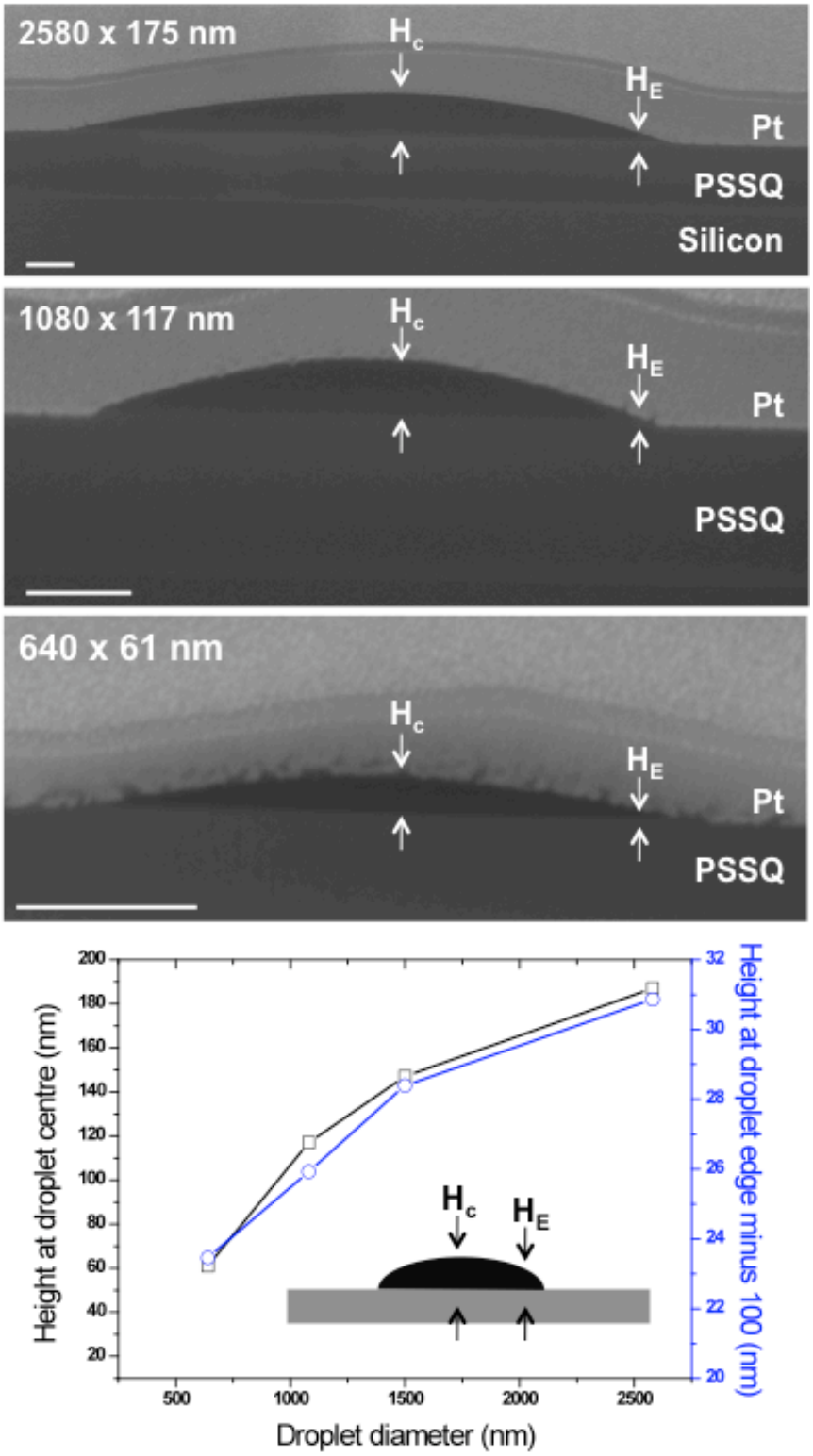

Figure 5: Tilt 54° SEM images post FIB cross sectioning of a (a) 2580 nm, (b) 1080 nm and (c) 640 nm microdroplets. (d) Height of droplet at centre as a function of changing microdroplet diameter. Height measurements are taken at (i) droplet centre and (ii) 100 nm in from the droplet edge to represent edge thickness. The scale bar is 200 nm for all images.

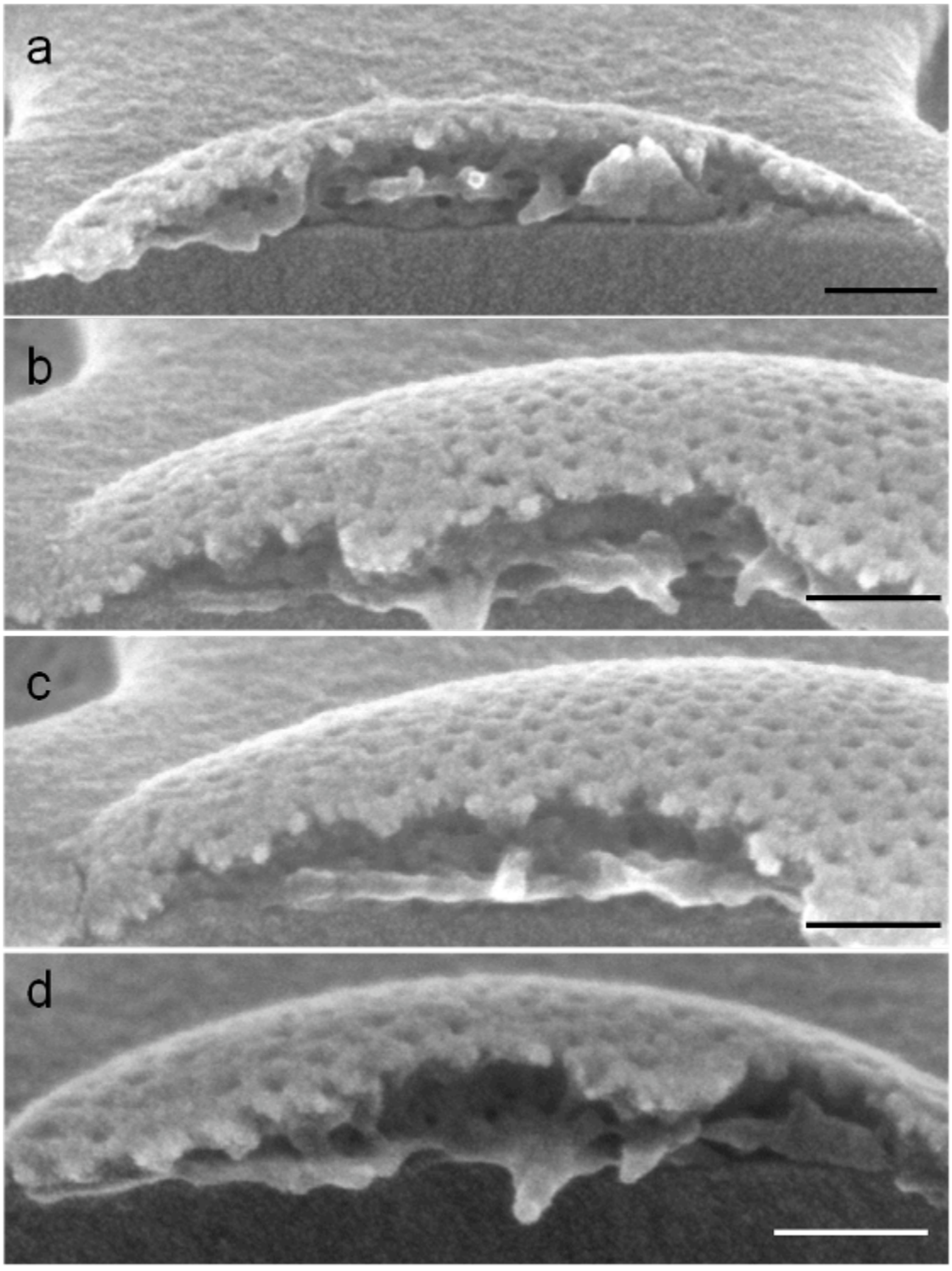

Figure 6: 70° tilt SEM images for 4 different 800 nm microdroplets sectioning by scribing to provide insight into the sub-surface orientation and morphology. The scale bar is 100 nm for all images.

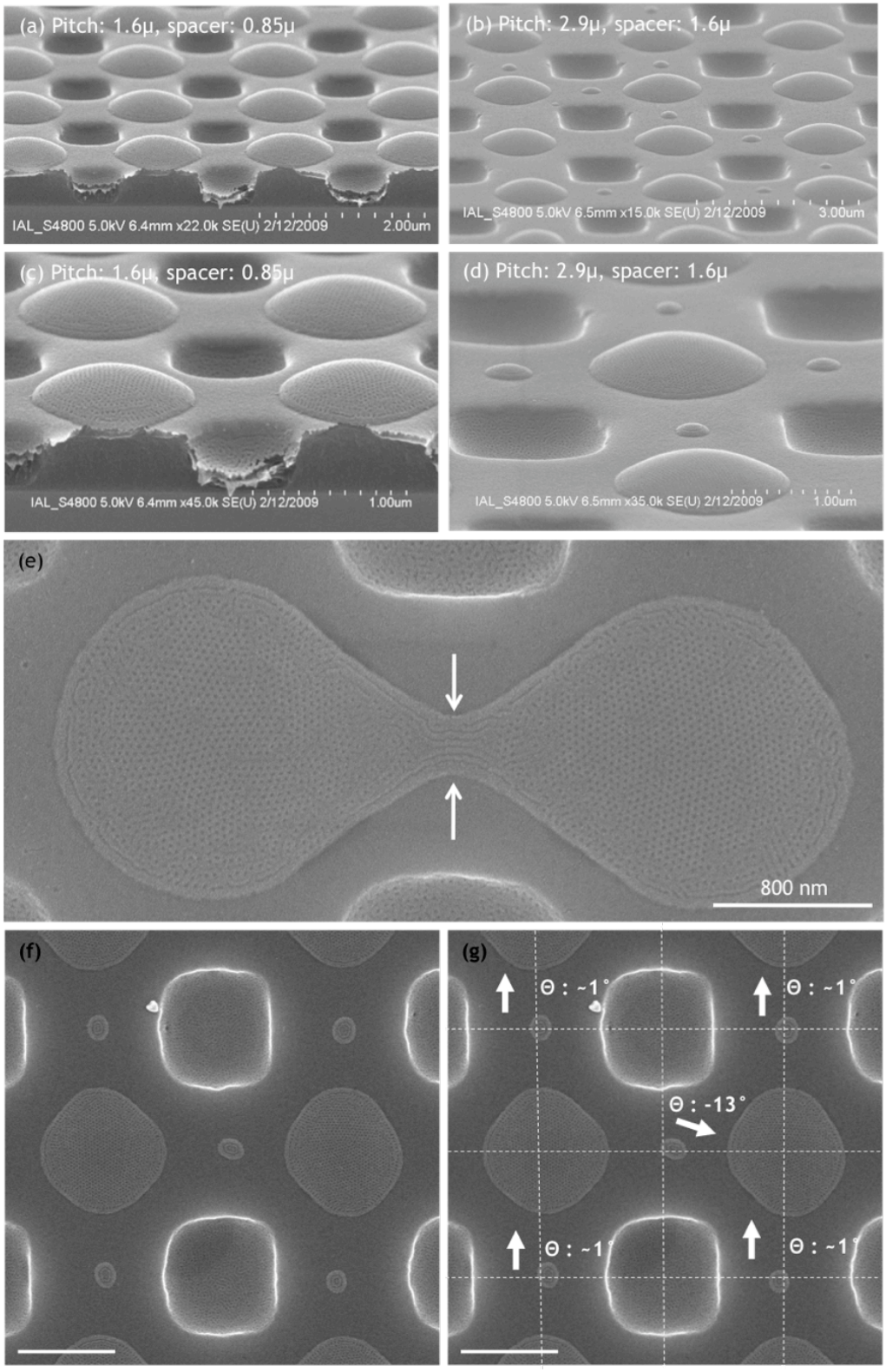

Figure 7: (a-d) 70° tilt SEM images of nano-ring formation by controlling the spacing between microdroplets. Images (c) and (d) are higher magnifications of (a) and (b). Error placement analysis for nanorings, (e) insight in dewetting mechanism by observing the formation of thin polymer ridges after annealing for 6 hrs highlighted by 2 arrows (f) top down SEM image of 5 nano-rings and (g) superimposed boundaries to emphasize *XY* positional and directionality error of the 5 nano-rings. The scale bar in image (e) is 800 nm and is 1000 nm in (f) and (g).

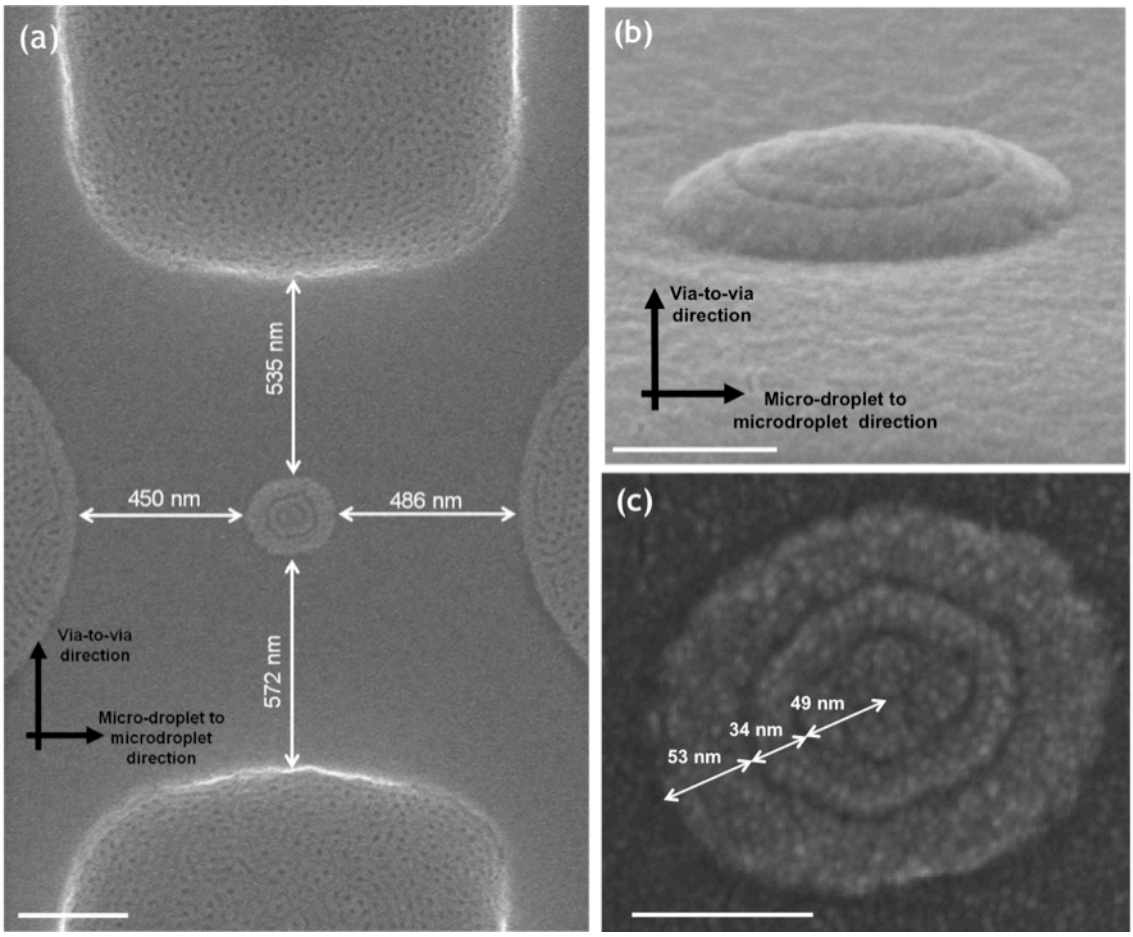

Figure 8: Aperiodic, self-aligned and self-supporting nano-rings of concentric parallel PMMA cylinders (a) top down and (b) 70° tilt SEM image of a nano-ring positioned between adjacent microdroplets and via holes, (c) high magnification top down SEM image of a nano-ring.

TOC graphic

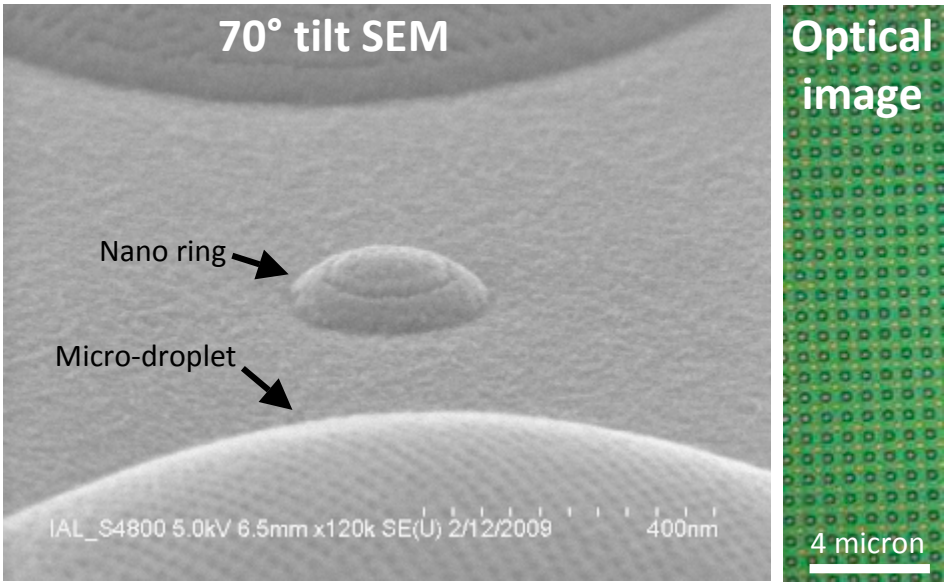

TOC graphic. (a) tilt SEM images of a nano-ring with concentric PMMA circles formed between two micro-droplets which have also undergone microphase separation facilitated by depositing PS-*b*-PMMA films on nano-imprinted PSSQ via hole arrays, (b) Optical image of a micro-droplet array (scale 4 micron)

Supporting information

Surface-directed dewetting of a nanostructured block copolymer for fabricating highly uniform nanostructured micro-droplets and concentric nano-rings

Richard A. Farrell[†,‡,ϕ,*], Nikolaos Kehagias[ϕ,§], Matthew T. Shaw[χ‡], Vincent Reboud[ϕ,§], Marc Zelsmann, Justin D. Holmes[†,‡,ϕ,], Clivia M. Sotomayor Torres[ϕ,§] and Michael A. Morris[†,‡,ϕ].

[†] Materials and Supercritical Fluid Group, Department of Chemistry, University College Cork, Cork, Ireland, [‡] Centre for Research on Adaptive Nanostructures and Nanodevices (CRANN), Trinity College Dublin, Dublin 2, Ireland. [ϕ] Micro-Nano centre, Tyndall National Institute, University College Cork, Cork, Ireland, [§]Catalan Institute of Nanotechnology, Campus de Bellaterra, Edifici CM7, ES 08193 – Bellaterra, Barcelona, Spain. Catalan Institute of Research and Advanced Studies ICREA, 08010 Barcelona, Spain. [χ] Intel Ireland limited, Collinstown Industrial estate, Leixlip, Co. Kildare, Ireland. Laboratoire des Technologies de la Microélectronique (CNRS), 38054 Grenoble, France. Current address: Department of Chemistry and Biochemistry, University of California Los Angeles, 607 Charles E. Young Drive East, Los Angeles, CA 90095-1569, USA.

*To whom correspondence should be addressed Tel: +1 310 794 6618; Fax, +1 310 794 6618; Email: r.farrell@chem.ucla.edu;

S1. Mixed orientation of cylinders in PSSQ NIL prepared templates

Figure S1 illustrates some of the experimental work carried out on aligning block copolymer in NIL prepared PSSQ templates. A mixed orientation of cylinders within the channel is observed across the patterns owing to the curvature of the trench, incommensurability and inappropriate wetting conditions. Figures 1b and 1e are FIB cross-sections of figures 1a and 1d which confirm the poor trench profile. Figures 1c and 1f are higher magnification images of mixed orientation of the PS-PMMA 46-21kg/mol. For this technique of aligning block copolymers in silsesquioxane patterns to work, the polymer must be able to access the brush layer at the base[1] (i.e. no residual layer) and the trench must also be of certain width, where beyond this width, defects will be permitted to occur within the channels[2]. Preliminary commensurability studies were also hampered by the fact that the base of the trench has a rounded profile, but more importantly the mixed orientation makes it difficult to differentiate either row spacing or cylinder spacing. Based on SEM images, we observe that no half cylinders are formed because PMMA does wet the sidewall. In certain regions were cylinders were arranged parallel to the base, 11 rows of parallel cylinders translate across the 450 nm trench. In a symmetric wetting scenario, 11 rows of cylinders would occupy a trench width of 440 nm. The fact that the trench was wide enough to allow defects creep in, added to the fact that the trench was 25% bigger than ideal width will ultimately lead to defective patterns[2]. The target width for this trench was 440 nm so optimisation of the NIL process or compensation for this fidelity loss must be included in future work.

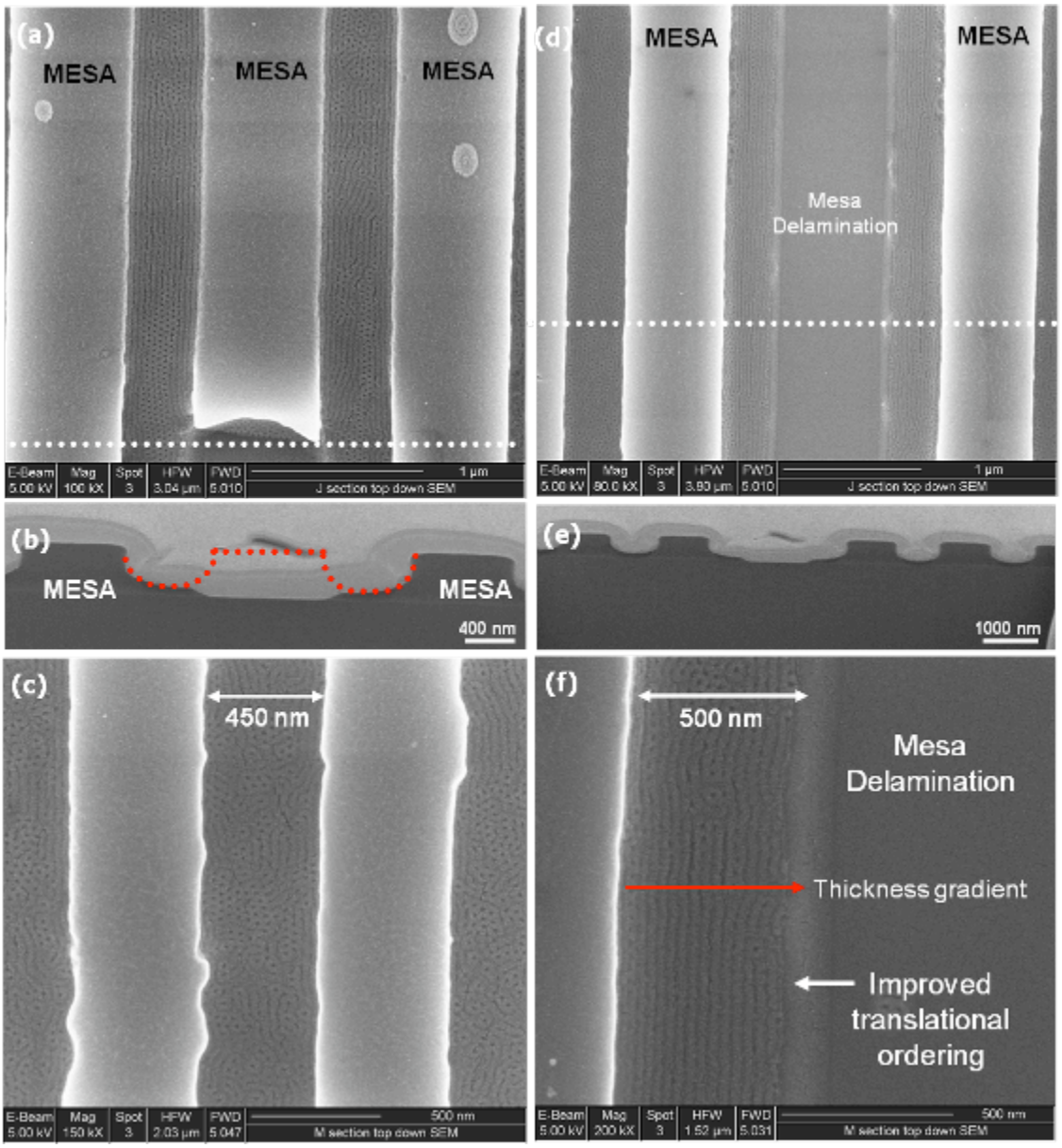

S1: (a), (c), (d) and (f) PS-*b*-PMMA pattern formation within PSSQ rounded trenches and (b) and (d) are FIB cross sections of (a) and (d) respectively. Mixed orientation is observed in most cases where mesa is intact. Improved translational ordering is observed where the Mesa has delaminated as shown in figures (d) and (f) as a result a thickness gradient.

S2. Statistical measurement of the equilibrium distance.

Centre to centre periodicities for various droplet and thin film structures were calculated using the open source Image J software (http://rsbweb.nih.gov/ij/). To eliminate the majority of defects, mainly from re-orientaion effects and increase in the radius of curvature towards the preriphery, analysis was performed in the centre region (indicated by a white box) as shown in figure S2. For the 600 nm microdroplet array, 7 microdroplets were analysed.

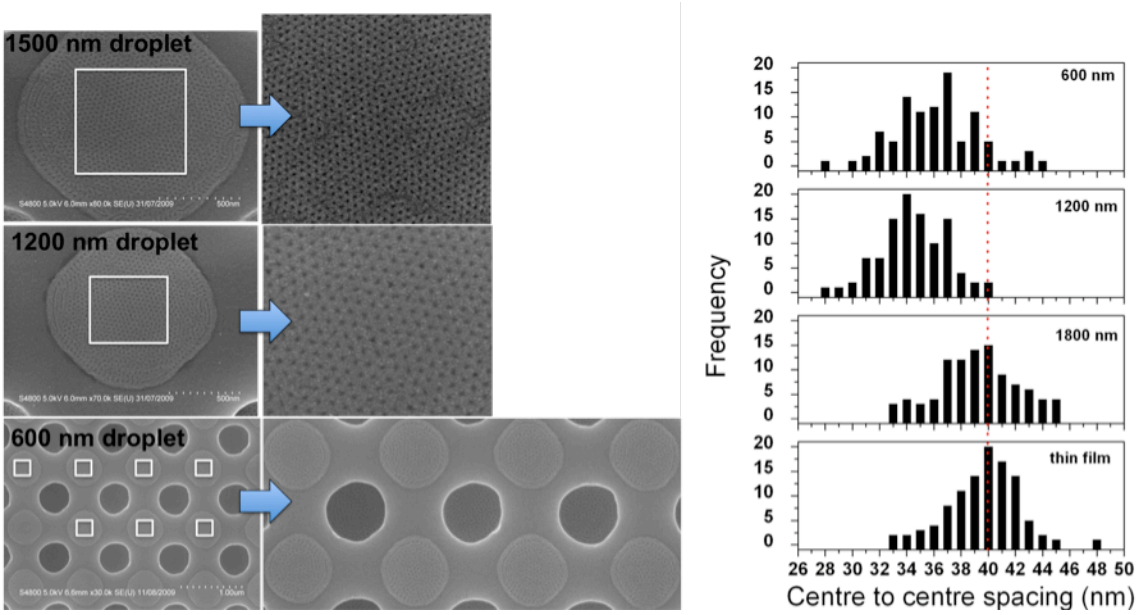

S2: Insight into dewetting process annealing at 6 hr

Supporting information references

(1) Yamaguchi, T.; Yamaguchi, H. *Advanced Materials* **2008**, *20*, 1684.

(2) Cheng J.Y.; Mayes A.M.; Ross C.A., *Nature Materials* **2004**, 3, 823-828

References

(1) Hamley, I. W. *Nanotechnology* **2003**, *14*, R39.

(2) Han, E.; Stuen, K. O.; Leolukman, M.; Liu, C. C.; Nealey, P. F.; Gopalan, P. *Macromolecules* **2009**, *42*, 4896.

(3) Thurn-Albrecht, T.; Schotter, J.; Kastle, C. A.; Emley, N.; Shibauchi, T.; Krusin-Elbaum, L.; Guarini, K.; Black, C. T.; Tuominen, M. T.; Russell, T. P. *Science* **2000**, *290*, 2126.

(4) Kim, H. C.; Russell, T. P. *Journal of Polymer Science Part B-Polymer Physics* **2001**, *39*, 663.

(5) Black, C. T.; Ruiz, R.; Breyta, G.; Cheng, J. Y.; Colburn, M. E.; Guarini, K. W.; Kim, H. C.; Zhang, Y. *Ibm Journal of Research and Development* **2007**, *51*, 605.

(6) Kim, S. O.; Solak, H. H.; Stoykovich, M. P.; Ferrier, N. J.; de Pablo, J. J.; Nealey, P. F. *Nature* **2003**, *424*, 411.

(7) Jung, Y. S.; Ross, C. A. *Nano Letters* **2007**, *7*, 2046.

(8) Li, H. W.; Huck, W. T. S. *Nano Letters* **2004**, *4*, 1633.

(9) Kim, S. H.; Misner, M. J.; Xu, T.; Kimura, M.; Russell, T. P. *Advanced Materials* **2004**, *16*, 226.

(10) Park, S.; Lee, D. H.; Xu, J.; Kim, B.; Hong, S. W.; Jeong, U.; Xu, T.; Russell, T. P. *Science* **2009**, *323*, 1030.

(11) Reiter, G. *Physical Review Letters* **1992**, *68*, 75.

(12) Reiter, G. *Langmuir* **1993**, *9*, 1344.

(13) Xie, R.; Karim, A.; Douglas, J. F.; Han, C. C.; Weiss, R. A. *Physical Review Letters* **1998**, *81*, 1251.

(14) Seemann, R.; Herminghaus, S.; Jacobs, K. *Journal of Physics-Condensed Matter* **2001**, *13*, 4925.

(15) Limary, R.; Green, P. F. *Langmuir* **1999**, *15*, 5617.

(16) Lu, G.; Li, W.; Yao, J. M.; Zhang, G.; Yang, B.; Shen, J. C. *Advanced Materials* **2002**, *14*, 1049.

(17) Zhang, Z. X.; Wang, Z.; Xing, R. B.; Han, Y. C. *Surface Science* **2003**, *539*, 129.

(18) Yoon, B. K.; Huh, J.; Kim, H. C.; Hong, J. M.; Park, C. *Macromolecules* **2006**, *39*, 901.

(19) Yoon, B.; Acharya, H.; Lee, G.; Kim, H. C.; Huh, J.; Park, C. *Soft Matter* **2008**, *4*, 1467.

(20) Mukherjee, R.; Bandyopadhyay, D.; Sharma, A. *Soft Matter* **2008**, *4*, 2086.

(21) Zhu, J. T.; Zhao, J. C.; Liao, Y. G.; Jiang, W. *Journal of Polymer Science Part B-Polymer Physics* **2005**, *43*, 2874.

(22) Lee, S. H.; Kang, H. M.; Kim, Y. S.; Char, K. *Macromolecules* **2003**, *36*, 4907.

(23) Hamley, I. W.; Hiscutt, E. L.; Yang, Y. W.; Booth, C. *Journal of Colloid and Interface Science* **1999**, *209*, 255.

(24) Carvalho, A. J. F.; Pereira-Da-Silva, M. A.; Faria, R. M. *European Physical Journal E* **2006**, *20*, 309.

(25) Croll, A. B.; Massa, M. V.; Matsen, M. W.; Dalnoki-Veress, K. *Physical Review Letters* **2006**, *97*.

(26) Croll, A. B.; Dalnoki-Veress, K. *European Physical Journal E* **2009**, *29*, 239.

(27) Hong, S. W.; Wang, J.; Lin, Z. *Angew. Chem. Int. Ed.* **2009**, *48*, 8356

(28) Xu, L.; Yu, X. F.; Shi, T. F.; An, L. J. *Soft Matter* **2009**, *5*, 2109.

(29) Kim, T. H.; Hwang, J.; Hwang, W. S.; Huh, J.; Kim, H. C.; Kim, S. H.; Hong, J. M.; Thomas, E. L.; Park, C. *Advanced Materials* **2008**, *20*, 522.

(30) Austin, M. D.; Ge, H. X.; Wu, W.; Li, M. T.; Yu, Z. N.; Wasserman, D.; Lyon, S. A.; Chou, S. Y. *Applied Physics Letters* **2004**, *84*, 5299.

(31) Chou, S. Y.; Krauss, P. R.; Renstrom, P. J. *Science* **1996**, *272*, 85.

(32) Bailey, T.; Choi, B. J.; Colburn, M.; Meissl, M.; Shaya, S.; Ekerdt, J. G.; Sreenivasan, S. V.; Willson, C. G. *Journal of Vacuum Science & Technology B* **2000**, *18*, 3572.

(33) Kehagias, N.; Reboud, V.; De Girolamo, J.; Chouiki, M.; Zelsmann, M.; Boussey, J.; Sotamayor-Torres, C. M. *Microelectronic Engineering* **2009**, *86*, 776.

(34) Namatsu, H.; Takahashi, Y.; Yamazaki, K.; Yamaguchi, T.; Nagase, M.; Kurihara, K. *Journal of Vacuum Science & Technology B* **1998**, *16*, 69.

(35) Kohl, A. T.; Mimna, R.; Shick, R.; Rhodes, L.; Wang, Z. L.; Kohl, P. A. *Electrochemical and Solid State Letters* **1999**, *2*, 77.

(36) Verschuuren, M.; van Sprang, H. *Mater. Res. Soc. Symp. Proc.* **2007**, *1002*, N03.

(37) Yamaguchi, T.; Yamaguchi, H. *Advanced Materials* **2008**, *20*, 1684.

(38) Cheng, J. Y.; Rettner, C. T.; Sanders, D. P.; Kim, H. C.; Hinsberg, W. D. *Advanced Materials* **2008**, *20*, 3155.

(39) Grigorescu, A. E.; Hagen, C. W. *Nanotechnology* **2009**, *20*.

(40) Chuang, V. P.; Ross, C. A.; Bilalis, P.; Hadjichristidis, N. *Acs Nano* **2008**, *2*, 2007.

(41) Wilmes, G. M.; Durkee, D. A.; Balsara, N. P.; Liddle, J. A. *Macromolecules* **2006**, *39*, 2435.

(42) Subramani, A.; Geerpuram, D.; Domanowski, A.; Baskaran, V.; Medushko, V. *Physica C-Superconductivity and Its Applications* **2004**, *404*, 241.

(43) Park, S.; Wang, J.-Y.; Kim, B.; Russell, T. P. *Nano Lett*. **2008**, *8*, 1667.

(44) O'Driscoll, S. M.; O'Mahony, C. T.; Farrell, R. A.; Fitzgerald, T. G.; Holmes, J. D.; Morris, M. A. *Chemical Physics Letters* **2009**, *476*, 65.

(45) Bita, I.; Yang, J. K. W.; Jung, Y. S.; Ross, C. A.; Thomas, E. L.; Berggren, K. K. *Science* **2008**, *321*, 939.

(46) Coulon, G.; Daillant, J.; Collin, B.; Benattar, J. J.; Gallot, Y. *Macromolecules* **1993**, *26*, 1582.

(47) Mansky, P.; Russell, T. P.; Hawker, C. J.; Mays, J.; Cook, D. C.; Satija, S. K. *Physical Review Letters* **1997**, *79*, 237.

(48) Wu, S. *Marcel Dekker Inc.: New York* **1982**.

(49) Black, C. T. *Applied Physics Letters* **2005**, *87*.

(50) Jeong, S. J.; Kim, J. E.; Moon, H. S.; Kim, B. H.; Kim, S. M.; Kim, J. B.; Kim, S. O. *Nano Letters* **2009**, *9*, 2300.

(51) Mansky, P.; Liu, Y.; Huang, E.; Russell, T. P.; Hawker, C. J. *Science* **1997**, *275*, 1458.

(52) Huang, E.; Russell, T. P.; Harrison, C.; Chaikin, P. M.; Register, R. A.; Hawker, C. J.; Mays, J. *Macromolecules* **1998**, *31*, 7641.

(53) Ryu, D. Y.; Ham, S.; Kim, E.; Jeong, U.; Hawker, C. J.; Russell, T. P. *Macromolecules* **2009**, *42*, 4902.

(54) Aissou, K.; Kogelschatz, M.; Baron, T. *Nanotechnology* **2009**, *20*.

(55) Aissou, K.; Kogelschatz, M.; Baron, T.; Gentile, P. *Surface Science* **2007**, *601*, 2611.

(56) Ruiz, R.; Kang, H. M.; Detcheverry, F. A.; Dobisz, E.; Kercher, D. S.; Albrecht, T. R.; de Pablo, J. J.; Nealey, P. F. *Science* **2008**, *321*, 936.

(57) Kobayashi, H. *Makromolekulare Chemie-Macromolecular Chemistry and Physics* **1993**, *194*, 2569.

(58) Welander, A. M.; Nealey, P. F.; Cao, H.; Bristol, R. *Journal of Vacuum Science & Technology B* **2008**, *26*, 2484.

(59) Suh, H. S.; Kang, H. M.; Liu, C. C.; Nealey, P. F.; Char, K. *Macromolecules* **2010**, *43*, 461.

(60) Knoll, A.; Horvat, A.; Lyakhova, K. S.; Krausch, G.; Sevink, G. J. A.; Zvelindovsky, A. V.; Magerle, R. *Physical Review Letters* **2002**, *89*.

(61) Crivello, J. V.; Malik, R. *Journal of Polymer Science Part a-Polymer Chemistry* **1997**, *35*, 407.